Brownian motor with time-delayed feedback

Dan Wu and Shiqun Zhu*

School of Physical Science and Technology, Suzhou University, Suzhou, Jiangsu 215006, People's Republic of China
(Received 25 September 2005; revised manuscript received 27 February 2006; published 16 May 2006)

An inertial Brownian motor with time-delayed feedback driven by an unbiased time-periodic force is investigated. It is found that the mean velocity and the rectification efficiency are decreased when the noise intensity is increased. While the shape of the mean velocity and the rectification efficiency can be changed from one peak to two peaks when the time delay is increased, the symmetry in the velocity probability distribution function is broken when the delay time is increased.

I. INTRODUCTION

In recent years, the stochastic systems with the time-delayed feedback have been investigated both theoretically and experimentally [1–18]. The properties of the time delay on the systems have been extensively discussed, for example, stochastic resonance with delayed interactions [19–22], synchronized and coordinated movements with time delay [23–25], laser systems with optical feedback [26–33], feedback-regulated voltage-controlled oscillators [34–37], etc. In these systems, the time delay arises mainly due to a finite transmission speed of matter, energy, and information.

Though the study of the noise-induced transport of Brownian motors has been widely investigated [38–41], much attention on ratchet has been focused on the way of the directed current [42] and the maximum of the efficiency [43]. However, in most of the previous investigations on Brownian motors, the time-delayed feedback is not included in the systems. Meanwhile, the efficiency is confined to the Brownian motor with external force F and based on the ratio of the work done by the particle against the external load and the input power [44–47]. Recently, the notion of the rectification efficiency is presented to discuss the efficiency in the absence of the external bias forces [48,49]. Thus, the Brownian motors with the time-delayed feedback need to be investigated. The effects of the time delay on the transport and the efficiency of the Brownian motors deserve further discussion.

In this paper, an inertial Brownian motor with time-delayed feedback driven by an unbiased monochromatic time-periodic force is investigated. In Sec. II, the theoretical model of the inertial Brownian motor with the time-delayed feedback is presented. In Sec. III, the effects of the noise intensity and the time delay on the mean velocity and the rectification efficiency are discussed. In Sec. IV, the effects of the time delay on the velocity probability distribution are investigated. In Sec. V, a wider range of the delay time and the driving frequency are analyzed. A discussion concludes the paper.

---

*Corresponding author. Electronic address: szhu@suda.edu.cn

II. A BROWNIAN MOTOR WITH TIME-DELAYED FEEDBACK

A Brownian motor with time-delayed feedback driven by an unbiased time-periodic force follows the Langevin equation [42,43]

$$\ddot{x}(t) + \gamma \dot{x}(t) = -V'(x(t-\tau)) + a\cos(\omega t) + \sqrt{2\gamma D_0}\xi(t),$$

(1)

where the dot denotes the differentiation with respect to time t while the prime denotes the differentiation with respect to the variable $x(t-\tau)$. The parameters a and ω are the strength and the angular frequency of the external force, γ is the friction coefficient and D_0 is the noise intensity, and $\xi(t)$ is the Gaussian white noise with zero mean and variance $\langle\xi(t)\xi(s)\rangle = \delta(t-s)$. In above equation, all the variables are rescaled and dimensionless.

The asymmetric ratchet potential $V(x(t-\tau))$ with time-delayed feedback is given by

$$V(x(t-\tau)) = V_0[a_0\sin(2\pi x(t-\tau)) + a_1\sin(4\pi x(t-\tau))$$
$$+ a_2\sin(6\pi x(t-\tau))],$$

(2)

where a_0, a_1, and a_2 are the coefficients representing the spatial asymmetry of the potential with $a_0 > a_1 > a_2$. These
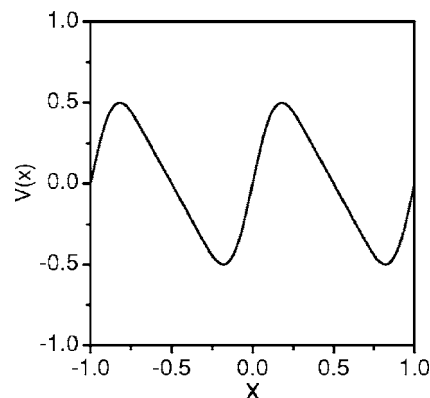

FIG. 1. The dimensionless potential $V(x)$ is plotted as a function of x. The parameters are dimensionless and are chosen as $V_0 = 0.461$, $a_0 = 1$, $a_1 = 0.245$, $a_2 = 0.04$. The force corresponding to this potential ranges between -4.67 and 1.83 [49].
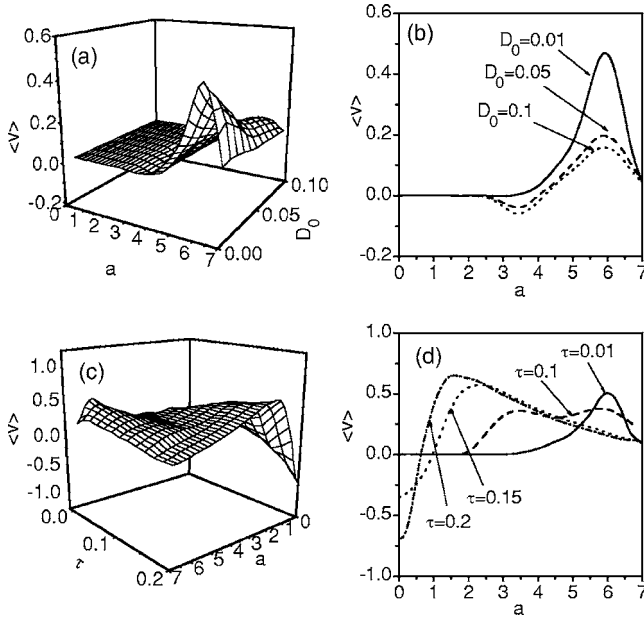
FIG. 2. The mean dimensionless velocity $\langle v \rangle$ of a delayed Brownian motor is plotted as a function of the driving force strength a, the white noise strength D_0, and the delay time τ. The parameters are dimensionless and are chosen as $V_0 = 0.461$, $\gamma = 0.9$, $\omega = 4.9$. (a) Three-dimensional plot of $\langle v \rangle$ as functions of a and D_0 when $\tau = 0.01$. (b) The mean velocity $\langle v \rangle$ as a function of a when $\tau = 0.01$ and D_0 is varied. (c) Three-dimensional plot of $\langle v \rangle$ as functions of a and τ when $D_0 = 0.01$. (d) The mean velocity $\langle v \rangle$ as a function of a when $D_0 = 0.01$ and τ is varied.
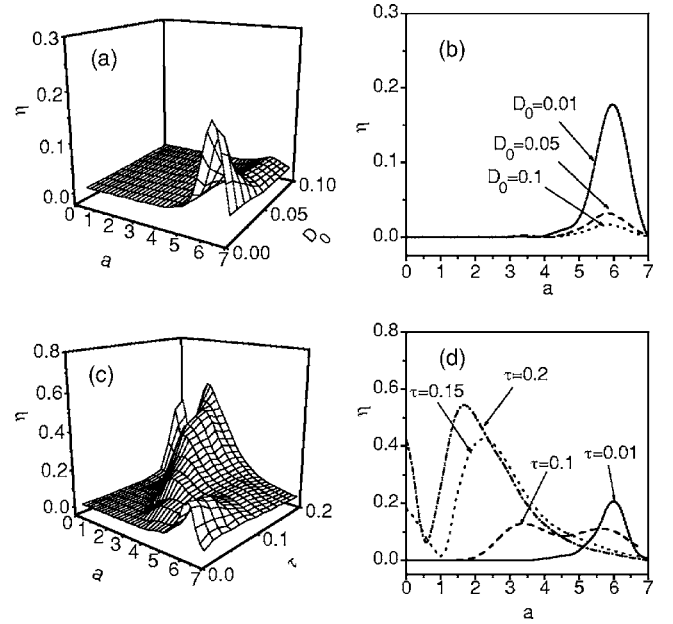

FIG. 3. The dimensionless rectification efficiency η of a delayed Brownian motor is plotted as a function of a, D_0, and τ. The parameters are dimensionless and are chosen as $V_0 = 0.461$, $\gamma = 0.9$, $\omega = 4.9$. (a) Three-dimensional plot of η as functions of a and D_0 when $\tau = 0.01$. (b) The efficiency η as a function of a when $\tau = 0.01$ and D_0 is varied. (c) Three-dimensional plot of η as functions of a and τ when $D_0 = 0.01$. (d) The efficiency η as a function of a when $D_0 = 0.01$ and τ is varied.

coefficients are chosen as $a_0 = 1$, $a_1 = 0.245$, and $a_2 = 0.04$ in the following discussions.

When there is no time delay with $\tau = 0$, the potential in Eq. (2) can be reduced to $V(x) = V_0[a_0 \sin(2\pi x) + a_1 \sin(4\pi x) + a_2 \sin(6\pi x)]$. This potential shape is composed of three spatial higher harmonics. The potential $V(x)$ as a function of x is plotted in Fig. 1. The natural direction of the Brownian motor motion corresponding to the potential is toward to the negative direction of x, in the direction of the weaker slope of the potential [49].

In the most common definition, the efficiency of a Brownian motor yields the result that the efficiency assumes zero when there is no external force. The rectification efficiency η, a new definition of the efficiency, is given by the ratio of the dissipated power $\gamma \langle v \rangle^2$ associated with the directed motion of the Brownian motor against the friction, and the input power from the load forcing [48,49]. It is applicable even if the external load is absent. The explicit equation of η can be written as

$$\eta = \frac{\langle v \rangle^2}{|\langle v^2 \rangle - D_0|}. \tag{3}$$

Since there is no analytic solutions that can be obtained from Eq. (1), only numerical computations are performed.

III. MEAN VELOCITY AND RECTIFICATION EFFICIENCY

The mean velocity $\langle v \rangle$ and the rectification efficiency η are analyzed by integrating Eqs. (1)–(3). The Euler method is used in the numerical calculations with a time step of $\Delta t = 10^{-3}$. The initial condition of $x(t)$ is taken from a uniform distribution over the dimensionless period $L = 1$ of the ratchet potential and the initial condition of $v(t)$ is chosen at random from a symmetric, uniform distribution over the interval $[-1, 1]$. The data obtained were averaged over 500 different trajectories and each trajectory evolved over 4.5×10^4 periods.

The mean velocity $\langle v \rangle$ as a function of the driving force strength a, the white noise strength D_0, and the delay time τ is plotted in Fig. 2. Figures 2(a) and 2(b) are plots of $\langle v \rangle$ as functions of a and D_0. From Figs. 2(a) and 2(b), it is seen that for small value of D_0, the Brownian motor reaches the maximum speed at about $a \simeq 6.0$. When D_0 is increased, the maximum speed is reduced and the reversal of the directed current appears. The mean speed reaches its negative extreme at about $a \simeq 3.4$. When D_0 is increased further, the negative extreme at $a \simeq 3.4$ is increased and the positive maximum at $a \simeq 6.0$ is decreased. It is seen that the motion of the Brownian motor is bounded when the driving force is small with $a < 2.5$. The inertial Brownian motor predominantly dwells in a potential well even when the noise disturbance is present. The averaged directed current is very small due to the fact that the escape jumps between the neighbor-
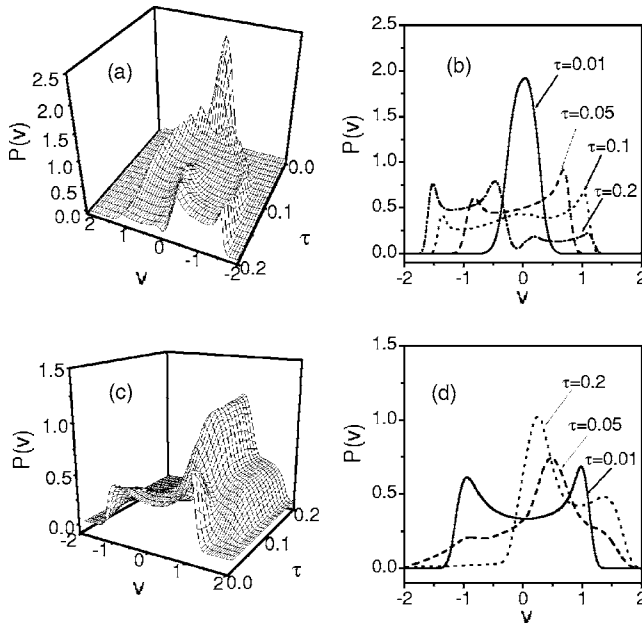
FIG. 4. The dimensionless velocity probability distribution $P(v)$ is plotted as a function of the velocity v and the delay time τ. The parameters are dimensionless and are chosen as $V_0=0.461$, $\gamma=0.9$, $\omega=4.9$, $D_0=0.01$. (a) Three-dimensional plot of $P(v)$ as functions of v and τ when $a=0$. (b) The velocity distribution $P(v)$ as a function of v when $a=0$ and τ is varied. (c) Three-dimensional plot of $P(v)$ as functions of v and τ when $a=2.5$. (d) The velocity distribution $P(v)$ as a function of v when $a=2.5$ and τ is varied.

FIG. 5. The dimensionless phase portrait of the system. The parameters are dimensionless and are chosen as $V_0=0.461$, $a_0=1$, $a_1=0.245$, $a_2=0.04$, $\gamma=0.9$, and $D_0=0.01$. (a) and (b): The phase portrait when $a=0$. (a) $\tau=0$; (b) $\tau=0.2$. (c) and (d): The phase portrait when $a=2.5$. (c) $\tau=0$; (d) $\tau=0.2$.

ing wells are rare. The input energy is transferred to the kinetic energy of the intrawell motion and finally dissipates. When the driving force is increased for $a>2.5$, the Brownian motor generates the directed transport behavior. It is seen that the noise disturbance may enhance the directional motion of the particle to the weaker slope of the potential and yield negative current. The negative current is increased when the noise disturbance D_0 is increased. When the driving force exceeds the upper threshold amplitude of the ratchet force at $a\simeq4.66$, the Brownian motor begins to move towards positive value of x, reaching the maximum speed near $a\simeq6.0$. Above this driving strength, the averaged velocity begins to decrease because of the weakening influence of the ratchet potential [49]. It seems that the negative velocity is caused by the noise disturbance; the increased noise disturbance may reduce the mean positive velocity and increase the mean negative velocity.

Figures 2(c) and 2(d) are the plots of $\langle v \rangle$ as functions of a and τ. From Figs. 2(c) and 2(d), it is seen that there is a single peak in $\langle v \rangle$ for small τ. The peak is located at about $a\simeq6.0$. The curve of $\langle v \rangle$ is changed from one peak to two peaks when τ is increased. The two peaks in $\langle v \rangle$ are located at about $a\simeq3.0$ and $a\simeq6.0$. When τ is increased, the two peaks in $\langle v \rangle$ are reduced to one peak again. The position of the peak in $\langle v \rangle$ is located at small value of a. When τ is increased further, the height of the peak is increased and the position of the peak is shifted to smaller value of a. Meanwhile, the reversal of the directed current appears. There is a negative extreme in $\langle v \rangle$ close to $a=0$. The negative extreme

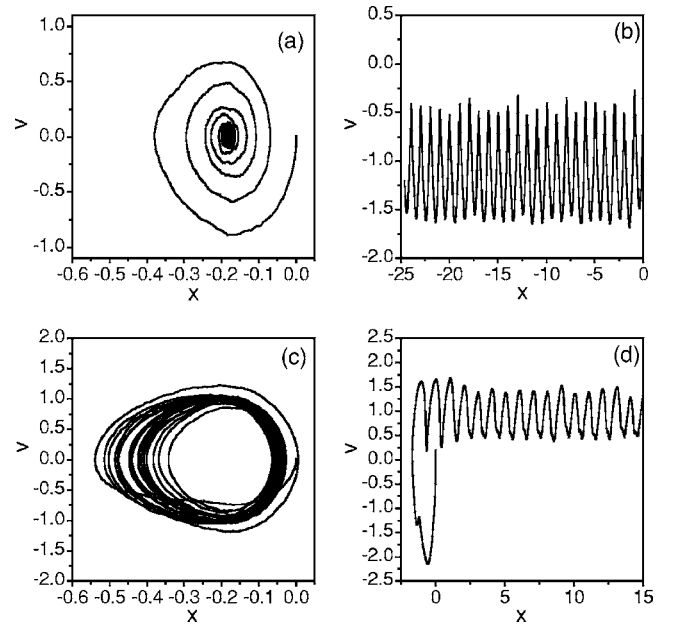in $\langle v \rangle$ is increased as τ is increased. It is clear that the time delay in the potential can induce rich phenomena in the mean velocity of the Brownian motor. For small delay time, there are single or two peaks in $\langle v \rangle$ of positive current. When the driving force strength is small, the inertial Brownian motor predominantly dwells in a potential well with very small negative velocity. The increased delay time may enhance the particle to move left, which leads to the increased negative current at $a=0$. When the driving force strength is increased, the increase of the delay time may stimulate the particle to move towards both directions. For large delay time, the positive peak in $\langle v \rangle$ is shifted to a small value of driving force and a negative peak appears close to $a=0$. It is seen that the particle may move towards the negative direction of x with large delay time even though there is no external load force. Thus, the particle with larger delay time may reach both maximum negative and positive speeds at smaller driving force strength.

The rectification efficiency η as a function of the driving force strength a, the white noise strength D_0, and the delay time τ is plotted in Fig. 3. Figures 3(a) and 3(b) are the plots of η as functions of a and D_0. From Figs. 3(a) and 3(b), it is seen that there is a major peak located at $a\simeq6.0$ in the curve of η. The height of the peak is decreased as D_0 is increased. There is a tiny peak located at $a\simeq3.4$. It seems that the rectification efficiency of the delayed Brownian motor is decreased with increasing value of the noise strength D_0.

Figures 3(c) and 3(d) are the plots of η as functions of a and τ. From Figs. 3(c) and 3(d), it is seen that the curve of η are changed from single peak to two peaks when the delay time τ is increased. For small value of τ, there is a peak
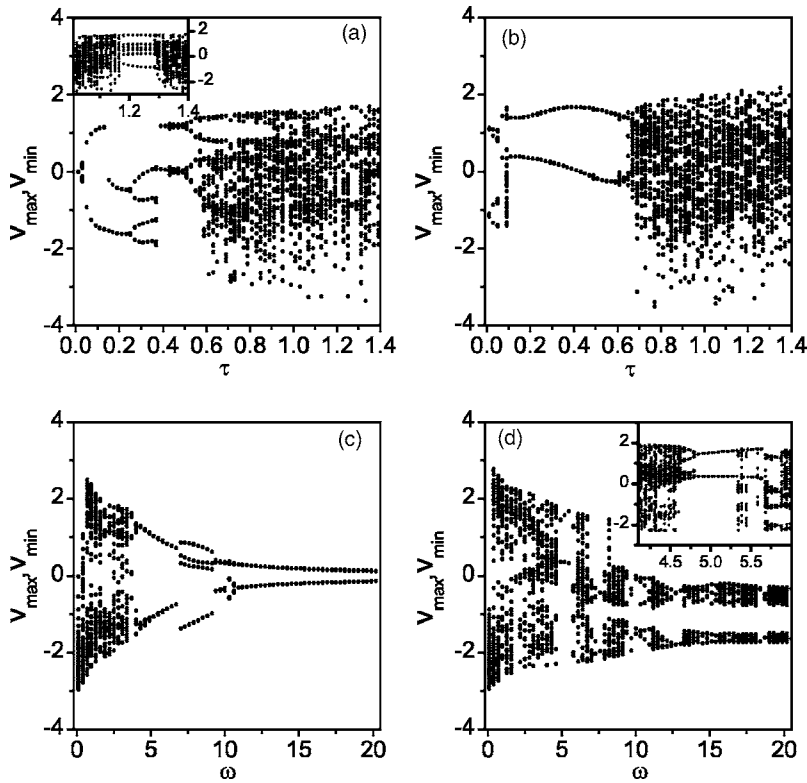
FIG. 6. The dimensionless deterministic bifurcation diagrams of the velocity v are plotted as a function of the delay time τ and the angular frequency ω of the driving force. The parameters are dimensionless and are chosen as $V_0=0.461$, $a_0=1$, $a_1=0.245$, $a_2=0.04$, $\gamma=0.9$, $D_0=0$. (a) and (b): The bifurcation diagrams as a function of τ when $\omega=4.9$ for different values of a. (a) $a=0$; (b) $a=2.5$. (c) and (d): The bifurcation diagrams as a function of ω when $a=2.5$ for different values of τ. (c) $\tau=0$; (d) $\tau=0.2$.

located at about $a\simeq6.0$. As τ is increased, there appears a second peak at a smaller value of a and the height of the peak at $a\simeq6.0$ is decreased. As τ is increased further, the height of the peak at a small value of a is increased and the peak at $a\simeq6.0$ disappears. There appears another maximum efficiency at $a=0$. It can be seen that the maximum efficiency of the delayed Brownian motor can be increased with increasing value of τ. This may provide a profound way to modify the delayed Brownian motor in order to obtain high efficiency even when there is no external driving force.

Compared with the average velocity in Fig. 2, similar shape in the rectification efficiency is obtained. The negative extreme in Fig. 2 becomes a positive peak in Fig. 3 due to the fact that the rectification efficiency defined by Eq. (3) is a function of $\langle v\rangle^2$ and is always greater than zero.

IV. VELOCITY PROBABILITY DISTRIBUTION

The velocity probability distribution function $P(v)$ is plotted in Fig. 4 as a function of the velocity v and the delay time τ.

When there is no driving force with $a=0$, the velocity probability distribution functions are plotted in Figs. 4(a) and 4(b) as functions of v and τ. From Figs. 4(a) and 4(b), it is seen that one peak in the curve of $P(v)$ is split to two peaks, then to three peaks, and finally to four peaks when τ is increased. The width of the curve is broadened and the asymmetry of the curve is enhanced as τ is increased. For small value of $\tau=0.01$, the curve of $P(v)$ is symmetrically distributed at two sides of $v=0$. However, the increasing value of τ breaks the symmetry of the curve of $P(v)$. Both the location and the height of the peaks in $P(v)$ is changed. When the

delay time is increased to $\tau=0.05$, one sharp peak in $P(v)$ is split to two lower peaks that are asymmetrically located at two sides of $v=0$. The peak at positive v is higher than that at negative v. The curve of $P(v)$ is broadened. When τ is increased to $\tau=0.1$, the two peaks in $P(v)$ are split to three peaks. The central peak is located at $v=0$. The curve of $P(v)$ is broadened further. The right peak is still higher than the left one. When τ is increased to $\tau=0.2$, the three peaks in $P(v)$ are split to four peaks located at two sides of $v=0$. The curve of $P(v)$ is broadened further. However, the two peaks located at negative v are much higher than that at positive v. It is seen that the velocity distribution $P(v)$ has concentrated mainly on one of the semiaxes for large delay time. Hence, the current arises mainly due to the asymmetry of the velocity distribution function even there is no external driving force.

When the driving force strength is $a=2.5$, the velocity probability distribution functions are plotted in Figs. 4(c) and 4(d) as functions of v and τ. From Figs. 4(c) and 4(d), it is seen that the asymmetry in the velocity distribution $P(v)$ is enhanced as τ is increased. For small value of $\tau=0.01$, there are two peaks in $P(v)$ distributed at $v=\pm1.0$. The right peak is higher and narrower than the left one. As τ is increased, the peak at the negative side of v is decreased while the peak at the positive side of v is increased. The location of the peak at the positive side of v is shifted to a small value of v. The whole curve is broadened. As τ is increased further, the peak at the negative side of v disappears and two peaks at the positive side of v appear. The two peaks at the positive side of v are increased as τ is increased. The major peak is located near $v=0$. The width of the curve $P(v)$ is also reduced. It is seen that the increasing delay time τ can enhance the

asymmetry and sharpness in $P(v)$ and thus increase the current. It is also clear that the velocity distribution $P(v)$ has concentrated mainly on the positive axis of v due to effect of the external load force and the increase of the delay time.

V. EFFECTS OF DELAYED TIME AND DRIVING FORCE

For a better understanding of the action of the time delay feedback and the driving force, the phase portrait and the deterministic bifurcation of the system need to be investigated.

The phase portraits of v versus x of the system are plotted in Fig. 5. In Figs. 5(a) and 5(b), the phase portraits are plotted when there is no driving force with $a=0$. In Fig. 5(a), there is no time delay with $\tau=0$. From Fig. 5(a), it is seen that the particle is initially located near $x=0$ and then moves towards negative x with decreased velocity magnitude $|v|$. Then the velocity is reduced to zero and the particle dwells in the potential well at $x\approx-0.2$. In Fig. 5(b), the time delay is $\tau=0.2$. From Fig. 5(b), it is seen that the particle moves towards negative x with negative velocity. The velocity v oscillates between -0.25 and -1.75 quasi-periodically. It is clear that the time delay can stimulate the particle to move towards negative x quasi-periodically even though there is no driving force. In Figs. 5(c) and 5(d), the phase portraits are plotted when the driving force is $a=2.5$. In Fig. 5(c), there is no time delay with $\tau=0$. From Fig. 5(c), it is seen that the particle is initially located near $x=0$ and then moves between $x=-0.6$ and $x=0$. The velocity v is bounded between $v=1.25$ and -1.25. In Fig. 5(d), the time delay is $\tau=0.2$. From Fig. 5(d), it is seen that the particle moves towards positive x under the influence of the driving force and the time delay. The velocity v oscillates between 1.75 and 0.25 after the transient of x from zero.

There are three different time scales inherent in the system, i.e., the intrinsic oscillation period without driving force given by $T_0=2\pi/(\text{Im }\lambda)$, where λ is the complex eigenvalue of the fixed point, the driving period $T=2\pi/\omega$, and the delay time τ. Though there is no analytic expression of the complex eigenvalue λ, it can be numerically calculated through Eq. (1). The numerical value of λ (for $D_0=a=\tau=0$) is given by $\lambda=-p\pm iq\approx-0.3\pm i5.0$. It would be interesting to look at a wider range of values of τ through the bifurcation diagrams of v_{max} and v_{min}. Here, v_{max} and v_{min} are the maximum and the minimum values of the velocity, respectively.

The bifurcation diagram of the deterministic system as a function of the delay time τ and the angular frequency ω of the driving force is plotted in Fig. 6. The bifurcation as a function of τ is plotted in Figs. 6(a) and 6(b). In Fig. 6(a), there is no driving force with $a=0$. From Fig. 6(a), it is seen that the particle moves with regular velocity when $\tau<0.55$. When $\tau>0.55$, the motion of the particle is chaotic. However, around $\tau\approx T_0\approx1.26$, there is a window that the particle moves with regular velocity again. This is clearly shown in the inset of Fig. 6(a). In Fig. 6(b), the driving force is $a=2.5$. From Fig. 6(b), it is seen that the motion of the particle is regular when $\tau<0.6$. When $\tau>0.6$, the motion is chaotic. There are no special features when $\tau\approx T_0\approx T$. It

seems that the driving force can enhance the chaotic motion of the particle. The bifurcation diagrams as a function of the angular frequency ω of the driving force are plotted in Figs. 6(c) and 6(d) when the driving force is $a=2.5$. In Fig. 6(c), there is no time delay with $\tau=0$. It is seen that the motion of the particle is chaotic when $\omega<q\approx5.0$. When $\omega>q$, the motion is regular. When ω is very large, the velocity of the particle tends to zero. In Fig. 6(d), the time delay is $\tau=0.2$. It is clear that the motion of the particle is chaotic at most values of ω. However, the motion is regular at these windows of $\omega\sim(1+n/2)q$, where $n=0,1,2,\ldots$. The first window that the regular motion appears is around $4.75<\omega<5.25$. This is shown in the inset of Fig. 6(d). It is seen that the delay time can enhance the chaotic motion of the particle but can keep the regularity at windows around $\omega\sim(1+n/2)q$.

VI. DISCUSSION

The effects of the noise strength and the delay time on the mean velocity and rectification efficiency of a Brownian inertial motor driven by an unbiased monochromatic time-periodic force are investigated. It is found that the mean velocity and the rectification efficiency are decreased when the value of white noise intensity D_0 is increased. When the delay time τ is increased, both the height and the number of peaks in the velocity and the efficiency can be varied. It is very interesting to note that the symmetry of the velocity distribution is broken when the value of delay time τ is increased. That is, the delay time can induce asymmetry in the velocity probability distribution function and increase the current and the efficiency in the system.

Recently, some simple models of time-delay feedback control of noise-induced oscillations have been investigated [4,5]. The analytical tools of mean-field approximation were developed for delay-differential equations, such as for the Van de Pol system. It is found that the modulation of some features with delay time τ has been associated with the local stability (eigenmodes) of the fixed point. The regularity of the noise-induced motion can be either increased or decreased by choosing proper value of time delay. The analytical tools [4,5,7–10] are difficult to apply in the model of Eq. (1). However, some similar features [4,5] have also been found in the Brownian motor with time-delayed feedback presented in this paper. When there is no driving force with $a=0$, the time delay can stimulate the particle to move towards negative direction. The regular motion of the particle appears for small delay time and appears again when the delay time is close to the intrinsic period T_0. For large delay time, the motion of the particle is chaotic. While there is a driving force, the time delay can induce positive motion of the particle. The delay time can enhance the chaotic motion but can keep the regularity when the driving frequency ω is close to $(1+n/2)$ of the intrinsic oscillation frequency q.

[1] J. W. Ryu, W. H. Kye, S. Y. Lee, M. W. Kim, M. Choi, S. Rim, Y. J. Park, and C. M. Kim, Phys. Rev. E **70**, 036220 (2004).

[2] S. Guillouzic, I. L'Heureux, and A. Longtin, Phys. Rev. E **61**, 4906 (2000).

[3] Y. J. Li, X. Lu, and J. Zhang, Phys. Rev. E **66**, 046501 (2002).

[4] N. B. Janson, A. G. Balanov, and E. Schöll, Phys. Rev. Lett. **93**, 010601 (2004).

[5] J. Pomplun, A. Amann, and E. Schöll, Europhys. Lett. **71**, 366 (2005).

[6] W. H. Kye, M. Choi, S. Rim, M. S. Kurdoglyan, C.-M. Kim, and Y.-J. Park, Phys. Rev. E **69**, 055202(R) (2004).

[7] T. D. Frank, P. J. Beek, and R. Friedrich, Phys. Rev. E **68**, 021912 (2003).

[8] T. D. Frank, Phys. Rev. E **66**, 011914 (2002).

[9] T. D. Frank, Phys. Rev. E **72**, 011112 (2005).

[10] T. Ohira and T. Yamane, Phys. Rev. E **61**, 1247 (2000).

[11] W. H. Kye, M. Choi, C. M. Kim, and Y. J. Park, Phys. Rev. E **71**, 045202(R) (2005).

[12] T. D. Frank, Phys. Rev. E **71**, 031106 (2005).

[13] D. Goldobin, M. Rosenblum, and A. Pikovsky, Phys. Rev. E **67**, 061119 (2003).

[14] A. Krawiecki and T. Stemler, Phys. Rev. E **68**, 061101 (2003).

[15] T. Ohira, Phys. Rev. E **55**, R1255 (1997).

[16] J. Houlihan, D. Goulding, Th. Busch, C. Masoller, and G. Huyet, Phys. Rev. Lett. **92**, 050601 (2004).

[17] H. Hasegawa, Phys. Rev. E **70**, 021911 (2004).

[18] S. Kunec and A. Bose, Phys. Rev. E **63**, 021908 (2001).

[19] H. Haken, Eur. Phys. J. B **18**, 545 (2000).

[20] S. Kim, S. H. Park, and H. B. Pyo, Phys. Rev. Lett. **82**, 1620 (1999).

[21] T. Ohira and Y. Sato, Phys. Rev. Lett. **82**, 2811 (1999).

[22] M. K. Stephen Yeung and S. H. Strogatz, Phys. Rev. Lett. **82**, 648 (1999).

[23] P. Tass, J. Kurths, M. G. Rosenblum, G. Guasti, and H. Hefter, Phys. Rev. E **54**, R2224 (1996).

[24] R. Engbert, C. Scheffczyk, R. T. Krampe, M. Rosenblum, J. Kurths, and R. Kliegl, Phys. Rev. E **56**, 5823 (1997).

[25] Y. Chen, M. Ding, and J. A. Scott Kelso, Phys. Rev. Lett. **79**, 4501 (1997).

[26] F. A. Hopf, D. L. Kaplan, H. M. Gibbs, and R. L. Shoemaker,

[27] H. M. Gibbs, F. A. Hopf, D. L. Kaplan, and R. L. Shoemaker, Phys. Rev. Lett. **46**, 474 (1981).

[28] F. T. Arecchi, G. Giacomelli, A. Lapucci, and R. Meucci, Phys. Rev. A **45**, R4225 (1992).

[29] I. Fischer, O. Hess, W. Elsässer, and E. Göbel, Phys. Rev. Lett. **73**, 2188 (1994).

[30] G. Giacomelli, R. Meucci, A. Politi, and F. T. Arecchi, Phys. Rev. Lett. **73**, 1099 (1994).

[31] B. Krauskopf, G. R. Gray, and D. Lenstra, Phys. Rev. E **58**, 7190 (1998).

[32] A. N. Pisarchik, R. Meucci, and F. T. Arecchi, Phys. Rev. E **62**, 8823 (2000).

[33] C. Masoller, Phys. Rev. Lett. **88**, 034102 (2002).

[34] W. Wischert, A. Wunderlin, A. Pelster, M. Olivier, and J. Groslambert, Phys. Rev. E **49**, 203 (1994).

[35] C. Simmendinger, A. Wunderlin, and A. Pelster, Phys. Rev. E **59**, 5344 (1999).

[36] M. Schanz and A. Pelster, Phys. Rev. E **67**, 056205 (2003).

[37] L. Larger, J. P. Goedgebuer, and T. Erheux, Phys. Rev. E **69**, 036210 (2004).

[38] J. Luczka, Physica A **274**, 200 (1999).

[39] P. Reimann, Phys. Rep. **361**, 57 (2002).

[40] R. D. Astumian and P. Hanggi, Phys. Today **55**, 33 (2002).

[41] P. Hanggi, F. Marchesoni, and F. Nori, Ann. Phys. **14**, 51 (2005).

[42] M. Kostur and J. Luczka, Phys. Rev. E **63**, 021101 (2001).

[43] J. M. R. Parrondo and B. J. Cisneros, Appl. Phys. A: Mater. Sci. Process. **75**, 179 (2002).

[44] R. Krishnan, M. C. Mahato, and A. M. Jayannavar, Phys. Rev. E **70**, 021102 (2004).

[45] N. Sanchez Salas and A. C. Hernändez, Phys. Rev. E **68**, 046125 (2003).

[46] H. Kamegawa, T. Hondou, and F. Takagi, Phys. Rev. Lett. **80**, 5251 (1998).

[47] B. Q. Ai, X. J. Wang, G. T. Liu, D. H. Wen, H. Z. Xie, W. Chen, and L.G. Liu, Phys. Rev. E **68**, 061105 (2003).

[48] D. Suzuki and T. Munakata, Phys. Rev. E **68**, 021906 (2003).

[49] L. Machura, M. Kostur, P. Talkner, J. Luczka, F. Marchesoni, and P. Hanggi, Phys. Rev. E **70**, 061105 (2004).

Phys. Rev. A **25**, 2172 (1982).